Lattice Mismatch in Crystalline Nanoparticle Thin Films

Citation: Gabrys, Paul A et al. "Lattice Mismatch in Crystalline Nanoparticle Thin Films." Nano Letters, 18, 1 (January 2018): 579-585 © 2018 The Author(s)

As Published: 10.1021/ACS.NANOLETT.7B04737

Publisher: American Chemical Society (ACS)

Persistent URL: https://hdl.handle.net/1721.1/127780

Version: Author's final manuscript: final author's manuscript post peer review, without publisher's formatting or copy editing

Lattice Mismatch in Crystalline Nanoparticle Thin Films

Paul A. Gabrys,[‡,†] Soyoung E. Seo,[‡,§,⊗] Mary X. Wang,[‡,⊥,⊗] EunBi Oh,[§,⊗] Robert J. Macfarlane,[,†] and Chad A. Mirkin[*,§,⊗,⊥,#]*

AUTHOR ADDRESS.

‡These authors contributed equally and are listed in alphabetical order.

†Department of Materials Science and Engineering, Massachusetts Institute of Technology (MIT), 77 Massachusetts Avenue, Cambridge, Massachusetts 02139, United States

§Department of Chemistry, ⊗International Institute for Nanotechnology, ⊥Department of Chemical and Biological Engineering, and #Department of Materials Science and Engineering, Northwestern University, Evanston, Illinois 60208, United States

*Address correspondence to chadnano@northwestern.edu (phone: 847-467-7302) and rmacfarl@mit.edu (phone: 617-715-2828)

ABSTRACT. For atomic thin films, lattice mismatch during heteroepitaxy leads to an accumulation of strain energy, generally causing the films to irreversibly deform and generate defects. In contrast, more elastically malleable building blocks should be better able to accommodate this mismatch and the resulting strain. Herein, that hypothesis is tested by utilizing

DNA-modified nanoparticles as "soft," programmable atom equivalents to grow a heteroepitaxial colloidal thin film. Calculations of interaction potentials, small angle X-ray scattering data, and electron microscopy images show that the oligomer corona surrounding a particle core can deform and rearrange to store elastic strain up to ±7.7% lattice mismatch, substantially exceeding the ±1% mismatch tolerated by atomic thin films. Importantly, these DNA-coated particles dissipate strain both elastically through a gradual and coherent relaxation/broadening of the mismatched lattice parameter and plastically (irreversibly) through the formation of dislocations or vacancies. These data also suggest that the DNA cannot be extended as readily as compressed, and thus the thin films exhibit distinctly different relaxation behavior in the positive and negative lattice mismatch regimes. These observations provide a more general understanding of how utilizing rigid building blocks coated with soft compressible polymeric materials can be used to control nano- and micro-structure.

KEYWORDS. Nanoparticle, Self-Assembly, Epitaxy, Thin Film, Lattice Mismatch

Heteroepitaxy is the process of depositing a thin film of one material atop a dissimilar material while maintaining the crystallinity of each composition. However, when the two lattice parameters are misaligned, significant strain is generated in the deposited crystals. In cases where there is minimal strain, the lattices form a coherent interface with a continuous crystallographic alignment. Unfortunately, in atomic thin films, only heteroepitaxial processes with a low lattice mismatch (max ±1%) tend to be coherent, and strain is instead generally alleviated by the formation of defects within the deposited crystal.[1–4] Since atoms behave like and are often modeled as hard spheres, engineering this crystal interface requires significant modulation of lattice composition (*e.g.* introducing dopant atoms to adjust lattice parameter). As a result, material composition must

often be compromised in order to prevent the formation of undesirable defects.[1] However, if a more elastically malleable building block was used, the equilibrium thin film crystal structures would be more accommodating of strain from lattice mismatch as a function of film thickness.[5,6]

While it is not possible to adjust an individual atom's "softness," programmable atom equivalents (PAEs) generated from rigid nanoparticles (NPs) and soft, highly tunable DNA ligand shells can be chemically adjusted in a deliberate and rational manner.[7–11] Indeed, such PAEs can be assembled into ordered, crystalline structures in a manner that is analogous to atomic crystallization.[12–14] We have previously shown that PAEs and lithographically defined templates can be used to grow single-crystalline thin films in an epitaxial manner.[15,16] In principle, this enables the study of epitaxy using building blocks that are more tunable than atoms. In this work, we extend this motif to the concept of heteroepitaxy by inducing controlled lattice mismatch between substrate and PAEs. While significant research effort has been devoted to investigating atomic heteroepitaxy,[2] PAEs have not been fully explored in this context yet. Understanding how strain is alleviated in these thin films is key to improving control over nano- and micro-scale structure in NP-based crystalline materials. This understanding could enable the fabrication of more complex nano-devices, particularly those requiring variations in NP composition with different lattice constants within the lattice.

In heteroepitaxial systems with lattice mismatch, elastic strain energy accumulates within the deposited thin film with the addition of each layer.[2,4] In atomic systems, all strain energy must be stored within the atomic bonds themselves, raising the overall potential energy of each individual building block. An oversimplified model can describe crystalline lattices as masses (atoms) connected by springs in each of the lattice directions. Each spring has an equilibrium length corresponding to an ideal interatomic spacing based on the energetics of binding and a spring

constant that opposes deviation.[17–19] Similarly, PAEs exhibit a well-defined, equilibrium interparticle distance that balances favorable DNA hybridization between neighbors with unfavorable steric repulsion between DNA coronae.[10,12,20,21] To an extent, PAEs can store elastic energy in different modes such as compression, extension, bending, and rearrangement of the DNA bonds between each set of neighboring PAEs, suggesting that they are significantly "softer" building blocks than atoms.[11,22,23] Given the numerous modes of elastic energy storage available to soft matter, we hypothesize that the PAE thin films will more readily accommodate any deviation due to lattice mismatch.

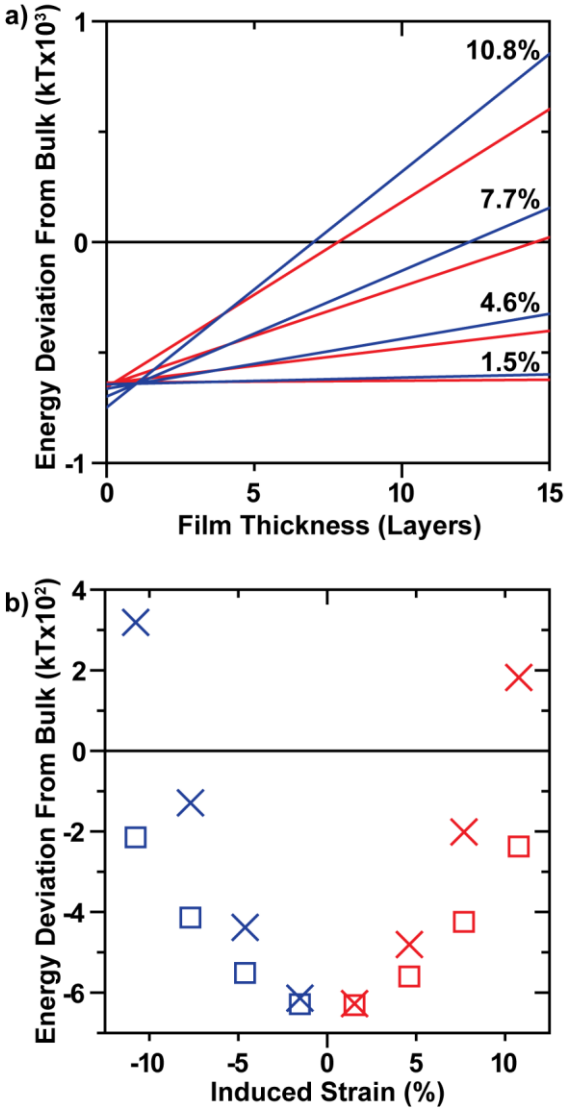

Figure 1. Modeled PAE thin films are energetically stable up to roughly ±9% lattice mismatch at 10 layers. Calculated PAE thin film potential energies relative to bulk a) as a function of film thickness and b) as a function of induced strain. In all figures, blue data correspond to negative lattice mismatch, red data to positive lattice mismatch; squares correspond to 5 layer samples, "X"s to 10 layers. Black lines correspond to "ideal" values.

To explore the energetic stability of a heteroepitaxial PAE thin film, a mathematical model based on mean field approximation[21] was used to calculate theoretical PAE interaction potential energies (Figure 1). These calculations used a PAE design consisting of 20 nm spherical gold NPs functionalized with one of two oligonucleotide sequences bound to linker strands with complementary "sticky ends" (Table S1). This binary system was assembled into body-centered cubic (bcc) crystals with an equilibrium lattice parameter of 65 nm. The foundation for this model is based on the assumptions that (i) all DNA sticky ends within the region of overlap between complementary PAEs are hybridized (Equation S1), and (ii) the PAEs are assembled into a rigid lattice with well-defined *x,y*-spacing (*i.e.* dissipation of strain energy was not considered). Previous studies show that the main thermodynamic contributor to lattice stability is the balance between attraction from DNA hybridization (Equation S2) and interparticle repulsion due to excluded volume interactions between the DNA brushes (Equations S3 and S4).[24–27] A "bulk" energy was first calculated by modeling a free-standing PAE film of a given thickness at the equilibrium lattice parameter. This is the energy associated with an unstrained lattice without the additional stability arising from being bound to a substrate. In the presence of a heterogeneous interface for the thin film cases, an interfacial energy term was included in the model by adding the attractive potential arising from the hybridization between a DNA-functionalized substrate and the superlattice (Supporting Information (SI) Section 1.3).

The impact of lattice mismatch on PAE thin film energy was investigated by calculating the potential energy of coherently assembled PAE thin films subjected to various amounts of lattice mismatch strain (Figure 1). The lattice energy calculations, compared to their bulk analogues, demonstrate that the soft DNA shell allows the assembled thin films to withstand a significant amount of strain. However, strain energy accumulates with each layer of the film and eventually destabilizes the overall structure to the point that the film is energetically less stable than the bulk state (Figure 1a). This also implies that at greater lattice mismatch the energy barrier for coherent, heteroepitaxial growth will be prohibitively high, resulting in incoherent growth. The model reveals that 10 layer films beyond roughly ±9% strain are less stable than their bulk analogue (Figure 1b). Thus, for the PAE design studied here, 10 layer thin films are predicted to only exhibit epitaxial alignment when the heterogeneous interface induces less than ±9% strain. Beyond this regime, the analytical model predicts that the accumulated strain energy will make thin film growth energetically unstable, favoring the formation of defects or dewetted amorphous (bulk) structures.

Scheme 1. Representation of the layer-by-layer PAE epitaxy platform and heteroepitaxial PAE thin films under negative (left) and positive (right) lattice mismatch (compressive and tensile strain, respectively) with coherent interfaces elastically relieving strain. Cross-section of the (001) plane is shown.

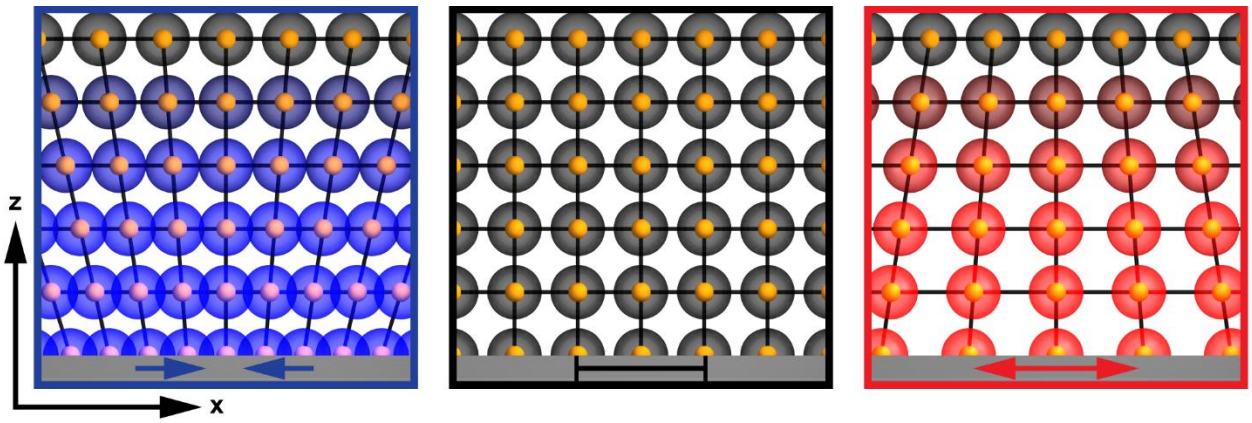

To investigate these hypotheses experimentally, PAEs consistent with the modeled design (DNA functionalized 20 nm gold NPs that can arrange in a bcc lattice with a 65 nm lattice parameter upon annealing) were synthesized following literature protocols[12,28] (SI Section 2, Table S1, Figures S2 and S3, and Equations S5 and S6). Arrays of gold dots commensurate in size with the PAEs were deposited on a silicon wafer in a pattern mimicking the (001) plane of the targeted bcc superlattice using electron beam lithography (SI Section 3.1). Once the dots were functionalized with one of the DNA strands and linkers (Table S1, SI Section 3.2), PAEs functionalized with the complementary sequence could bind and form a monolayer on the patterned array (Figure S4). Previous studies have shown that the PAEs bind to the dot array in the position that maximizes the number of DNA linkages.[15,16] In this case, the particle was driven to sit in the center of four dots, epitaxially continuing the patterned crystal plane (*i.e.* the formation of the (002) plane). This process was continued in a layer-by-layer fashion to assemble multiple layers on each template (Table S3). To study the phenomenon of heteroepitaxy and the impact of lattice mismatch, arrays were fabricated with different lattice parameters than the ideal bulk PAE superlattice (up to ±10.8% lattice mismatch, Table S2). The thin films were embedded in silica following established protocols[29] (SI Section 4.2) and the structure of each was determined by synchrotron-based

transmission small angle X-ray scattering (SAXS), as well as focused ion beam (FIB) cross-sectioning followed by scanning electron microscopy (SEM).

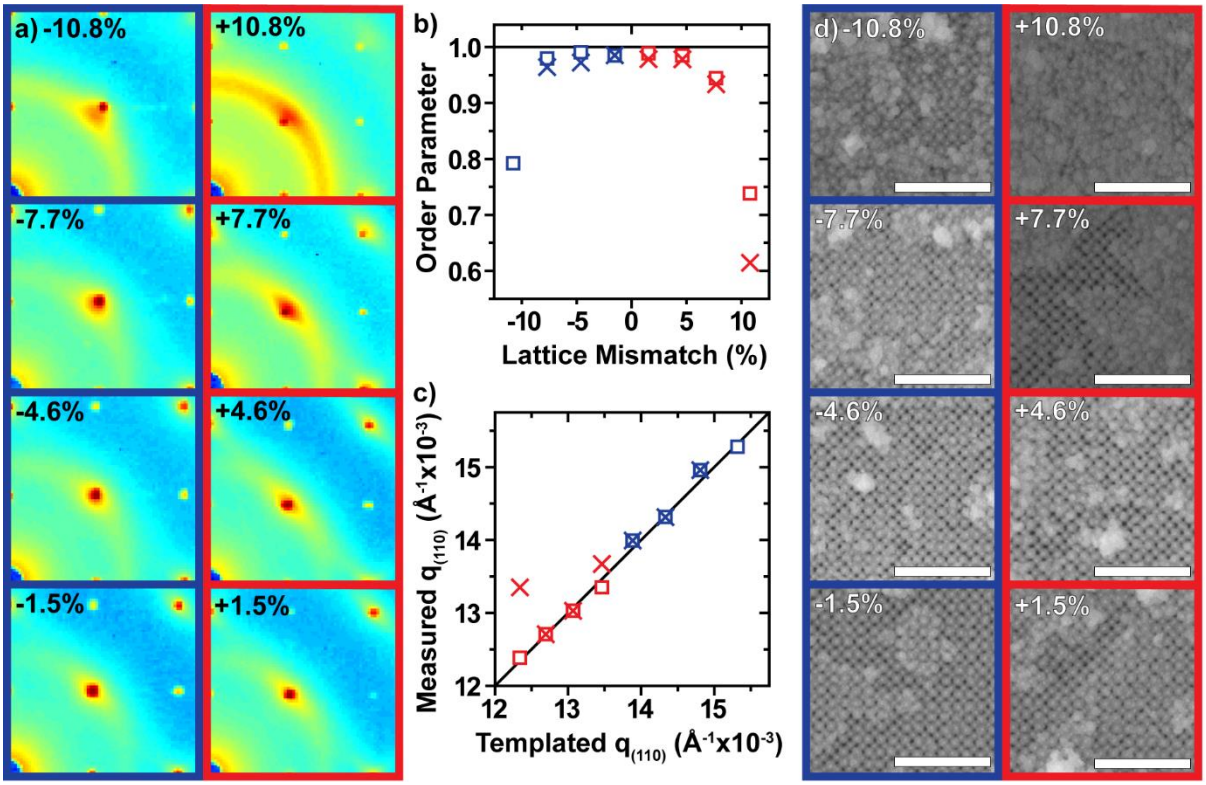

Figure 2. PAE thin films maintain coherency with the patterned crystallography up to ±7.7% lattice mismatch. a) 2D transmission SAXS data centered on the (110) reciprocal spot – 10 layer sample for all shown except -10.8% (5 layer) shown, b) order parameter – calculated by comparing the integrated intensity of the (110) spot to the intensity of the amorphous ring – as a function of lattice mismatch, c) the maximum $q_{(110)}$ value from the measured SAXS data compared to the templated $q_{(110)}$ position, and d) representative SEM micrographs of the thin film surface – 10 layer sample for all shown except -10.8% (5 layer) shown.

First, SAXS was used to determine the degree of crystallinity and epitaxy. Since the incident X-ray beam was normal to the substrate for these measurements, the resulting SAXS data shown in Figure 2 are 2D projections of the *x*,*y*-plane positions in reciprocal space. Each SAXS pattern

shows a high degree of single-crystalline ordering consistent with the patterned bcc (001) plane (Figure 2a). Full 2D images (Figure S6) and 1D circular averaging (Figure S7) for samples consisting of either 5 or 10 layers are available in the SI. In these data, epitaxially aligned PAEs contribute to the intensity of the reciprocal space lattice positions. Any deviation in alignment results in a broadening of each diffraction spot. Regions of non-epitaxial PAEs within the thin film add to the intensity of a diffuse ring encircling the beam center. Therefore, we can define an order parameter (Equation S8) by comparing the integrated SAXS intensity of a diffraction spot to the relative integrated intensity of the diffuse ring over the same q-range (Figure 2b). Consistent with both the hypotheses and the calculations of interaction potentials, all samples exhibit a reasonably high degree of order (intensity at the diffraction spot 2.5 times greater than the integrated intensity of the corresponding diffuse ring), even the cases of ±10.8% lattice mismatch. Within ±7.7%, the thin films exhibit near perfect ordering, matching the analytical model. This is in stark comparison to atomic thin film heteroepitaxy, which rarely remains epitaxial and coherent above ±1% lattice mismatch.[2] SAXS also confirms that the interparticle distance between PAEs in the thin film (calculated from the $q_{(110)}$ position, Equation S9) conform to the induced mismatch (Figure 2c). Finally, additional confirmation of the epitaxial alignment was achieved with SEM (Figures 2d and S5) and atomic force microscopy (Figure S11) of the thin films, which both show a transition from an aligned and ordered surface into an amorphous layer beyond ±7.7% mismatch.

The strong parallels between the modeled and experimental results indicate that a majority of the accumulated strain energy in this "soft" heteroepitaxy system is likely stored within the DNA shell. However, broadening of the diffraction spots (which increases with larger values of lattice mismatch) is indicative of deviation of PAEs from ideal lattice positions and suggests that some of the strain energy is being dissipated throughout the thin film structure. In general, a material

can alleviate strain energy in two ways: elastically or plastically. Elastic alleviation is strain removal that is done without breaking any bonds between individual building blocks, while plastic deformation requires the breaking of individual bonds and generally manifests in the form of defects.[3] Heteroepitaxial thin films (atomic or PAE-based) that can dissipate strain elastically largely do so through a gradual change of the interparticle distances in lattice planes further from the heterogeneous interface (Scheme 1). In other words, lattice planes further from the mismatched interface will have interparticle distances closer to the ideal. Atoms in a crystalline lattice have relatively rigid and directional atomic orbitals resulting in a sharp and deep energy well as a function of position. Therefore, atoms incur significant energetic penalties for deviating too readily from an ideal lattice position. At high lattice mismatch, the strain energy present in the bond between two atoms outweighs the energy cost of breaking that nearest neighbor bond, driving the atoms to rearrange their equilibrium structure and form defects like misfit dislocations or lattice vacancies.[3] The mechanisms of alleviating the strain from lattice mismatch available to heteroepitaxial PAE thin films can be deduced from their resulting, equilibrium structure. In contrast with atoms, spherical PAEs are isotropic and have omni-directional binding. Additionally, the flexibility of the DNA corona allows for a wider range of achievable binding distances at a lower energy cost.[11] Therefore, these "soft" building blocks are hypothesized to more readily allow for elastic alleviation of strain.

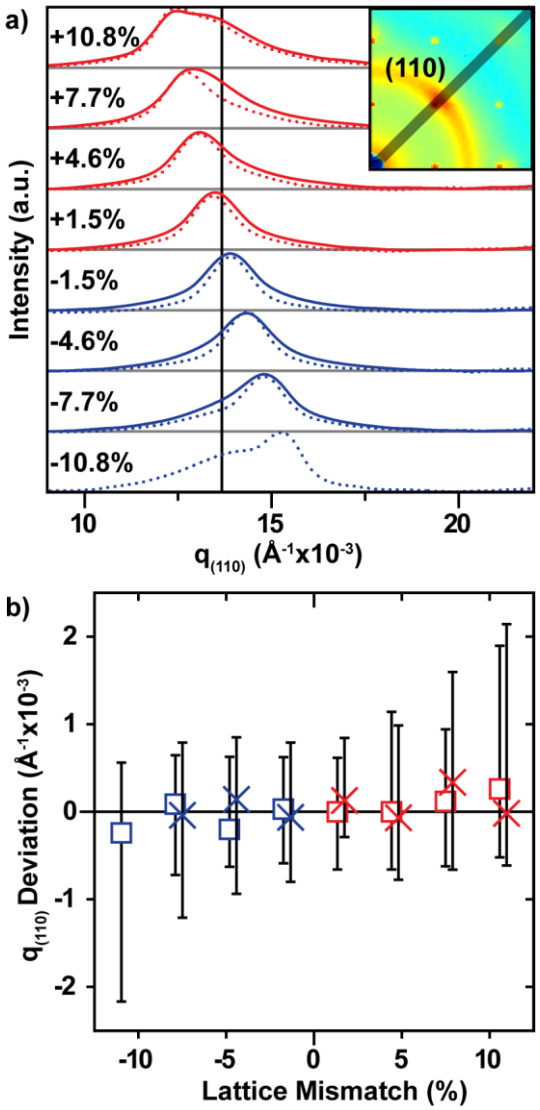

Figure 3. PAE thin films alleviate strain energy elastically in the *x,y*-plane through gradual retraction/expansion of interparticle distance toward the bulk value. a) 1D radial line averages of the SAXS data along the close-packed direction with the "ideal" bulk phase (110) peak position noted for reference. Dotted lines are 5 layer films and solid lines are 10 layers. Inset: representative schematic of direction and width of radial line cuts. b) Plot of max (110) peak positions relative to the template and the peak width at half max of each line cut in the high-*q* (small interparticle distance) and low-*q* (large interparticle distance) directions displayed as error bars.

Indeed, the SAXS data clearly reveal an elastic mode of strain relief (Figure 3). Intensities at larger scattering angles (larger q values) correspond to smaller real space distances, and vice versa. By averaging radially along *only* the 45° angle, trends in the average interparticle distance can be observed (Figures 3a and S8). In all mismatch cases, the (110) peak intensity is strongest where matched with the template position and exhibits a tail that leans toward the bulk, ideal interparticle spacing. Plotting the (110) peak maxima and their respective rightward and leftward peak widths at half max (Equations S10 and S11), the data demonstrate that when the thin films are compressed under negative lattice mismatch, the PAEs relax toward larger spacing and vice versa (Figure 3b). While this conclusion may be intuitive for soft matter in general, it highlights the behavior unique to a "soft" building block in the construction of crystalline materials.

While strain energy in these PAE systems is alleviated predominantly in an elastic manner by stretching or compressing soft DNA shells, plastic deformation would be expected to occur when the accumulated strain energy in the collective DNA "bond" between two particles exceeds the energy penalty associated with breaking that bond (*i.e.* the DNA ligand shell is too stretched or compressed for the DNA sticky end duplexes to remain in the hybridized state). Given the high grafting density of oligomers on the surface of the PAEs (which results in a crowded environment for the DNA strands)[30,31] and the fact that the DNA bonds consist almost entirely of duplexed DNA, we hypothesize that the DNA corona surrounding an individual particle will display different physical characteristics under compressive and tensile lattice mismatch. Specifically, under negative mismatch, the volume available to a PAE in the lattice is reduced, generally confining it to its local lattice position. However, under positive mismatch, the free accessible volume of each lattice site is increased, providing a larger space for each PAE to occupy. Thus, PAEs under positive lattice mismatch have higher degrees of translational freedom (variation

around ideal lattice sites) than films of a corresponding compressive mismatch. According to the analytical model in this work, an increased interparticle distance reduces the overlap region between complementary particles, leading to fewer DNA sticky end hybridization events and a higher overall energy. Therefore, the maximum number of DNA hybridization events may occur when the particle is shifted away from the lattice site, a behavior that is not considered in the model. By releasing entirely from one neighbor (breaking the "bond" between the two PAEs) and shifting toward its other complementary nearest neighbors, each PAE in a larger-than-ideal unit cell could increase its overall DNA hybridization, resulting in a lower equilibrium, lattice energy.

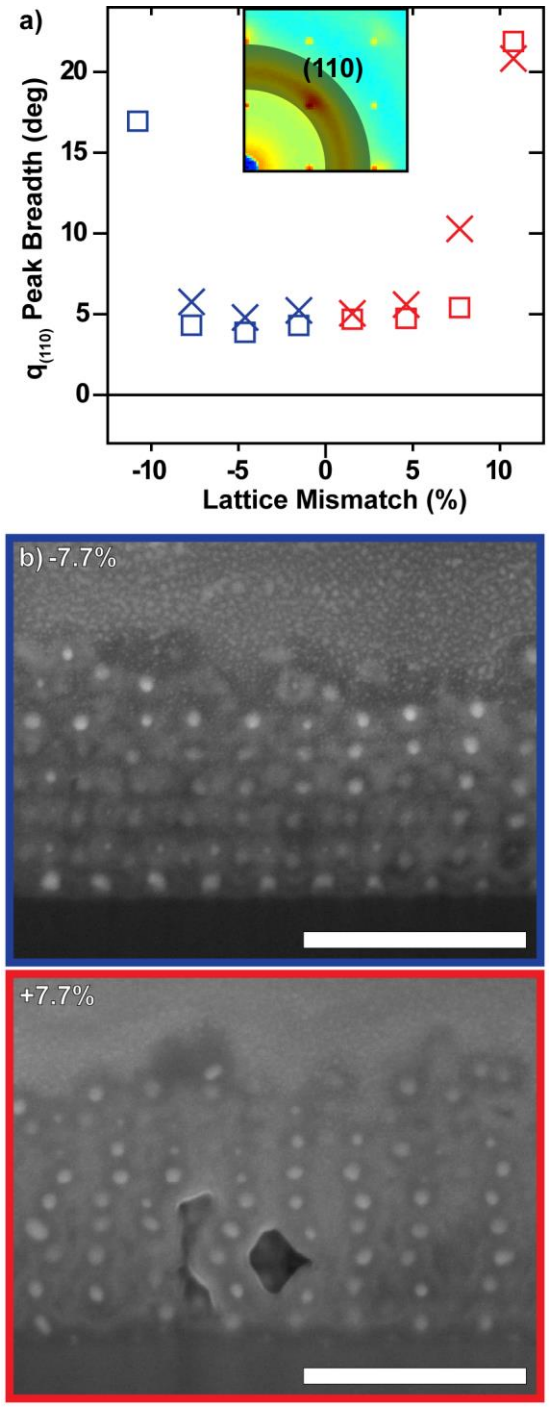

Figure 4. Plastic alleviation of strain in PAE thin films in the presence of high strain. a) Plot of relative breadth of the (110) SAXS peak in the azimuthal direction (corresponding to the degree of PAE translational freedom within the thin film) versus lattice mismatch. Inset: representative schematic of direction and width of azimuthal cuts. b) The higher frequency of random, lateral

deviations in *x,y*-planes under high positive lattice mismatch was verified visually from the FIB cross-sections. Scale bars are 250 nm.

This type of random, plastic deviation results in azimuthal, instead of radial, broadening of SAXS diffraction spots as the PAEs within the film transition from precise locations to more random, amorphous ones. After taking broad azimuthal cuts (from q-values of 0.0093 to 0.0183 $Å^{-1}$) that encompass the entirety of the (110) diffraction spot in each sample, the 1D averaged intensities were plotted as a function of angle (Figure S9); the relative breadth of these peaks (Equation S12) was then plotted to determine the degree of translational freedom for each sample (Figure 4a). As hypothesized, the tensile samples have a much higher degree of translational freedom. To corroborate this conclusion from the SAXS data, the 10 layer thin films were cross-sectioned via FIB milling and imaged with SEM. Each cross-section was aligned with the (001) plane of the thin film to readily observe any deviation in the PAE positions. The significant difference between translational freedom in the negative versus positive mismatch cases is visually apparent by observing the (001) planes moving in the z-direction in the representative FIB cross-sections comparing the +7.7% lattice mismatch sample to the -7.7% sample (Figure 4b). Similar to atomic materials under tensile strain,[3] the PAE films under positive lattice mismatch show signs of "micro-tears" (gaps) where void space within the structure is a result of PAEs locally breaking bonds in the same direction. The fact that these gaps are not observed in the negative mismatch samples indicates that the PAEs' "soft" coronae can be compressed with the addition of strain but not as readily stretched. This is consistent with prior experimental results on the mechanical properties of single DNA strands.[32–36] This non-reciprocal difference gives rise to the different physical characteristics and amounts of plastic versus elastic deformation of the PAE lattices under positive and negative lattice mismatch.

The microscopy images (full 15 μm cross-sections of each 10 layer thin film available in the SI) corroborate the broad conclusions of the SAXS data; all thin films appear, in general, epitaxial with increasing frequency of defects as mismatch increases. These defects culminate in the formation of large "glassy" regions under extreme mismatch. Under positive lattice mismatch, the defects are commonly random deviations in the spacing between lattice planes (Figure 4b). Interestingly, the FIB cross sections, particularly for the negative lattice mismatch films, also show the presence of other plastic deformation mechanisms to alleviate strain that are commonly observed in atomic systems.[1,2] These include both dislocations and vacancies, which alleviate strain by breaking bonds between particles and changing the local crystal structure of the lattice (Figure S10).

The conclusions presented here reveal the complexity of using PAEs as thin film building blocks. They exhibit remarkable strain tolerance based on their design, accommodating a lattice mismatch up to ±7.7% while maintaining coherency. Unlike atoms, PAEs are readily able to store the accumulated strain energy within the DNA bonds between particles and alleviate some of the strain elastically through a change in lattice parameter as a function of layer number. While the release of any strain in these PAE thin films is primarily elastic relaxation, these building blocks still undergo plastic defect formation. The observed misfit dislocations and vacancies are comparable to atomic thin films. In principle, these PAEs should be tunable to behave more like soft matter or more like hard sphere atoms depending on synthetic variation of the building block design and deposition parameters. "Soft" heteroepitaxy, while maintaining similarities to atomic heteroepitaxy, contains unique mechanistic differences that can greatly affect material synthesis. This effect might be even more prominent for crystals in solution, where macroscopic curvature could provide additional mechanisms for strain relief. In principle, the induced strain at the

interface could be used to control the thickness of overgrown material atop a dissimilar material with different lattice parameter, *i.e.* in a core-shell structure. Ultimately, this study yields unparalleled control over nano- and micro-structure in NP-based systems. The platform investigated in this work can provide a toolkit for novel NP devices requiring improved control over interparticle distances, as well as provide a proxy system for the study of interface/thin film science at the boundaries of heteroepitaxial interfaces.

ASSOCIATED CONTENT

AUTHOR INFORMATION

Corresponding Author

*Address correspondence to chadnano@northwestern.edu and rmacfarl@mit.edu

Author Contributions

The manuscript was written through contributions of all authors. All authors have given approval to the final version of the manuscript. ‡These authors contributed equally and are listed in alphabetical order.

Notes

The authors declare no competing financial interest. Any findings and conclusions expressed in this material are those of the authors and do not necessarily reflect the views of the National Science Foundation (NSF).

ACKNOWLEDGMENT

This work was supported by the following awards: Air Force Office of Scientific Research FA9550-16-1-0150 (oligonucleotide syntheses and purification), FA9950-17-1-0348 (DNA-

functionalization of gold nanoparticles), and FA9550-17-1-0288 Young Investigator Research Program (substrate fabrication, particle assembly and electron microscopy characterization); the Vannevar Bush Faculty Fellowship program sponsored by the Basic Research Office of the Assistant Secretary of Defense for Research and Engineering and funded by the Office of Naval Research through grant N00014-15-1-0043 (substrate functionalization); the Center for Bio-Inspired Energy Science, an Energy Frontier Research Center funded by the U.S. Department of Energy, Office of Science, Basic Energy Sciences award DE-SC0000989 (nanoparticle superlattice thin film assembly and characterization). Fabrication and SEM characterization were performed at the Materials Technology Laboratory at MIT. SAXS experiments were carried out at beamline 12-ID-B at the Advanced Photon Source, a U.S. DOE Office of Science User Facility operated by Argonne National Laboratory under Contract DE-AC02-06CH11357, and the authors particularly acknowledge the help of Byeongdu Lee. FIB was performed at the Shared Experimental Facilities in the Center for Materials Science and Engineering at MIT, supported in part by the MRSEC Program under National Science Foundation award DMR-1419807. AFM was performed at the Materials Research Center of Northwestern University supported by National Science Foundation award DMR-1121262. P.A.G. acknowledges support from the NSF Graduate Research Fellowship Program under grant NSF 1122374. S.E.S. acknowledges partial support from the Center for Computation and Theory of Soft Materials Fellowship. M.X.W. was supported by the NSF Graduate Research Fellowship.

Supporting Information. Experimental procedures, including interaction potential calculations, oligonucleotide sequences, nanoparticle functionalization and assembly, substrate preparation, characterization/analysis techniques (SEM, SAXS, FIB Cross-sectioning, and AFM), and FIB

cross-sections are available in the SI. The Supporting Information is available free of charge on the ACS Publications website.

REFERENCES

(1) Palmstrom, C. J. Epitaxy of Dissimilar Materials. *Annu. Rev. Mater. Sci.* **1995**, *25*, 389–415.

(2) Ohring, M. *Materials Science of Thin Films: Deposition and Structure*; 2nd ed.; Academic Press: San Diego, CA, 2002.

(3) Callister, W. D.; Rethwisch, D. G. *Materials Science and Engineering: An Introduction*; 8th ed.; John Wiley & Sons: Hoboken, NJ, 2010.

(4) Ayers, J. E.; Kujofsa, T.; Rago, P.; Raphael, J. *Heteroepitaxy of Semiconductors: Theory, Growth, and Characterization, Second Edition*; CRC Press: CT, 2016.

(5) Rupich, S. M.; Castro, F. C.; Irvine, W. T. M.; Talapin, D. V. Soft Epitaxy of Nanocrystal Superlattices. *Nat. Commun.* **2014**, *5*, 1-10.

(6) Van Blaaderen, A.; Ruel, R.; Wiltzius, P. Template-Directed Colloidal Crystallization. *Nature* **1997**, *385*, 321–324.

(7) Mirkin, C. A.; Letsinger, R. L.; Mucic, R. C.; Storhoff, J. J. A DNA-Based Method for Rationally Assembling Nanoparticles into Macroscopic Materials. *Nature* **1996**, *382*, 607–609.

(8) Hill, H. D.; Macfarlane, R. J.; Senesi, A. J.; Lee, B.; Park, S. Y.; Mirkin, C. A. Controlling the Lattice Parameters of Gold Nanoparticle FCC Crystals with Duplex DNA Linkers. *Nano Lett.* **2008**, *8*, 2341–2344.

(9) Park, S. Y.; Lytton-Jean, A. K. R.; Lee, B.; Weigand, S.; Schatz, G. C.; Mirkin, C. A. DNA-Programmable Nanoparticle Crystallization. *Nature* **2008**, *451*, 553–556.

(10) Nykypanchuk, D.; Maye, M. M.; van der Lelie, D.; Gang, O. DNA-Guided Crystallization of Colloidal Nanoparticles. *Nature* **2008**, *451*, 549–552.

(11) Senesi, A. J.; Eichelsdoerfer, D. J.; Brown, K. A.; Lee, B.; Auyeung, E.; Choi, C. H. J.; Macfarlane, R. J.; Young, K. L.; Mirkin, C. A. Oligonucleotide Flexibility Dictates Crystal Quality in DNA-Programmable Nanoparticle Superlattices. *Adv. Mater.* **2014**, *26*, 7235–7240.

(12) Macfarlane, R. J.; Lee, B.; Jones, M. R.; Harris, N.; Schatz, G. C.; Mirkin, C. A. Nanoparticle Superlattice Engineering with DNA. *Science* **2011**, *334*, 204–208.

(13) Auyeung, E.; Li, T. I. N. G.; Senesi, A. J.; Schmucker, A. L.; Pals, B. C.; de la Cruz, M. O.; Mirkin, C. A. DNA-Mediated Nanoparticle Crystallization into Wulff Polyhedra. *Nature* **2014**, *505*, 73–77.

(14) Macfarlane, R. J.; Lee, B.; Hill, H. D.; Senesi, A. J.; Seifert, S.; Mirkin, C. A. Assembly and Organization Processes in DNA-Directed Colloidal Crystallization. *Proc. Natl. Acad. Sci.* **2009**, *106*, 10493–10498.

(15) Wang, M. X.; Seo, S. E.; Gabrys, P. A.; Fleischman, D.; Lee, B.; Kim, Y.; Atwater, H. A.; Macfarlane, R. J.; Mirkin, C. A. Epitaxy: Programmable Atom Equivalents Versus Atoms. *ACS Nano* **2017**, *11*, 180–185.

(16) Hellstrom, S. L.; Kim, Y.; Fakonas, J. S.; Senesi, A. J.; Macfarlane, R. J.; Mirkin, C. A.; Atwater, H. A. Epitaxial Growth of DNA-Assembled Nanoparticle Superlattices on Patterned Substrates. *Nano Lett.* **2013**, *13*, 6084–6090.

(17) Fetter, A. L.; Walecka, J. D. *Theoretical Mechanics of Particles and Continua*; Courier Corporation: MA, 2003.
(18) Kittel, C. Introduction to Solid State Physics. *Am. J. Phys.* **1967**, *35*, 547–548.
(19) Born, M.; Huang, K. Dynamical Theory of Crystal Lattices. *Am. J. Phys.* **1955**, *23*, 474–474.
(20) Wang, M. X.; Brodin, J. D.; Millan, J. A.; Seo, S. E.; Girard, M.; Olvera de la Cruz, M.; Lee, B.; Mirkin, C. A. Altering DNA-Programmable Colloidal Crystallization Paths by Modulating Particle Repulsion. *Nano Lett.* **2017**, *17*, 5126–5132.
(21) Seo, S. E.; Li, T.; Senesi, A. J.; Mirkin, C. A.; Lee, B. The Role of Repulsion in Colloidal Crystal Engineering with DNA. *J. Am. Chem. Soc.* **2017**, *139,* 16528-16535.
(22) O'Brien, M. N.; Girard, M.; Lin, H.-X.; Millan, J. A.; Cruz, M. O. de la; Lee, B.; Mirkin, C. A. Exploring the Zone of Anisotropy and Broken Symmetries in DNA-Mediated Nanoparticle Crystallization. *Proc. Natl. Acad. Sci.* **2016**, *113*, 10485–10490.
(23) Lee, O.-S.; Cho, V. Y.; Schatz, G. C. A- to B-Form Transition in DNA Between Gold Surfaces. *J. Phys. Chem. B* **2012**, *116*, 7000–7005.
(24) Maye, M. M.; Nykypanchuk, D.; van der Lelie, D.; Gang, O. DNA-Regulated Micro- and Nanoparticle Assembly. *Small* **2007**, *3*, 1678–1682.
(25) Tkachenko, A. V. Morphological Diversity of DNA-Colloidal Self-Assembly. *Phys. Rev. Lett.* **2002**, *89*, 148303.
(26) Nykypanchuk, D.; Maye, M. M.; van der Lelie, D.; Gang, O. DNA-Based Approach for Interparticle Interaction Control. *Langmuir* **2007**, *23*, 6305–6314.
(27) Jin, R.; Wu, G.; Li, Z.; Mirkin, C. A.; Schatz, G. C. What Controls the Melting Properties of DNA-Linked Gold Nanoparticle Assemblies? *J. Am. Chem. Soc.* **2003**, *125*, 1643–1654.
(28) Hill, H. D.; Mirkin, C. A. The Bio-Barcode Assay for the Detection of Protein and Nucleic Acid Targets Using DTT-Induced Ligand Exchange. *Nat. Protoc.* **2006**, *1*, 324–336.
(29) Auyeung, E.; Macfarlane, R. J.; Choi, C. H. J.; Cutler, J. I.; Mirkin, C. A. Transitioning DNA-Engineered Nanoparticle Superlattices from Solution to the Solid State. *Adv. Mater.* **2012**, *24*, 5181–5186.
(30) Hurst, S. J.; Lytton-Jean, A. K. R.; Mirkin, C. A. Maximizing DNA Loading on a Range of Gold Nanoparticle Sizes. *Anal. Chem.* **2006**, *78*, 8313–8318.
(31) Hill, H. D.; Millstone, J. E.; Banholzer, M. J.; Mirkin, C. A. The Role Radius of Curvature Plays in Thiolated Oligonucleotide Loading on Gold Nanoparticles. *ACS Nano* **2009**, *3*, 418–424.
(32) Bustamante, C.; Bryant, Z.; Smith, S. B. Ten Years of Tension: Single-Molecule DNA Mechanics. *Nature* **2003**, *421*, 423–427.
(33) Rief, M.; Clausen-Schaumann, H.; Gaub, H. E. Sequence-Dependent Mechanics of Single DNA Molecules. *Nat. Struct. Mol. Biol.* **1999**, *6*, 346–349.
(34) Marko, J. F.; Cocco, S. The Micromechanics of DNA. *Phys. World* **2003**, *16*, 37.
(35) Bustamante, C.; Smith, S. B.; Liphardt, J.; Smith, D. Single-Molecule Studies of DNA Mechanics. *Curr. Opin. Struct. Biol.* **2000**, *10*, 279–285.
(36) Kosikov, K. M.; Gorin, A. A.; Zhurkin, V. B.; Olson, W. K. DNA Stretching and Compression: Large-Scale Simulations of Double Helical structures. *J. Mol. Biol.* **1999**, *289*, 1301–1326.

TABLE OF CONTENTS GRAPHIC

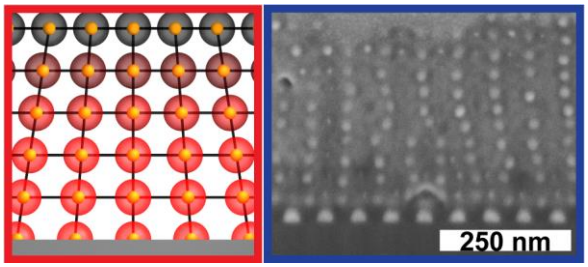

for TOC only